AIP Advances

# Illumination angle and layer thickness influence on the photo current generation in organic solar cells: A combined simulative and experimental study

Jan Mescher, Adrian Mertens, Amos Egel, Siegfried W. Kettlitz, Uli Lemmer, and Alexander Colsmann

Citation: AIP Advances **5**, 077188 (2015); doi: 10.1063/1.4928074
View online: http://dx.doi.org/10.1063/1.4928074
View Table of Contents: http://scitation.aip.org/content/aip/journal/adva/5/7?ver=pdfcov
Published by the AIP Publishing



# Illumination angle and layer thickness influence on the photo current generation in organic solar cells: A combined simulative and experimental study

Jan Mescher,[1,a] Adrian Mertens,[1] Amos Egel,[1] Siegfried W. Kettlitz,[1] Uli Lemmer,[1,2] and Alexander Colsmann[1,b]
[1]*Light Technology Institute (LTI), Karlsruhe Institute of Technology (KIT), Engesserstraße 13, D-76131 Karlsruhe, Germany*
[2]*Institute of Microstructure Technology (IMT), Karlsruhe Institute of Technology (KIT), Hermann-von-Helmholtz-Platz 1, D-76344 Eggenstein-Leopoldshafen, Germany*

(Received 14 April 2015; accepted 25 July 2015; published online 31 July 2015)

In most future organic photovoltaic applications, such as fixed roof installations, facade or clothing integration, the solar cells will face the sun under varying angles. By a combined simulative and experimental study, we investigate the mutual interdependencies of the angle of light incidence, the absorber layer thickness and the photon harvesting efficiency within a typical organic photovoltaic device. For thin absorber layers, we find a steady decrease of the effective photocurrent towards increasing angles. For 90-140 nm thick absorber layers, however, we observe an effective photocurrent enhancement, exhibiting a maximum yield at angles of incidence of about 50°. Both effects mainly originate from the angle-dependent spatial broadening of the optical interference pattern inside the solar cell and a shift of the absorption maximum away from the metal electrode.  [http://dx.doi.org/10.1063/1.4928074]

Key features of organic photovoltaic devices are their printability and mechanical flexibility[1–3] and hence their applicability on curved or flexible surfaces on building facades or clothing.[4,5] On curved surfaces and in static applications, however, organic solar cells (OSCs) mostly receive sunlight under varying angles. Therefore, good absorption of diffuse light is important and impacts on the device design.[6] Optical simulations have been used to phenomenologically predict the angle-dependent optoelectronic device properties of OSCs.[7–10]

In this work, we develop a fundamental understanding of the impact of the active layer thickness on the angle-dependent light absorption. By a combined experimental and numerical study utilizing the polymeric absorber poly[[2,6′-4,8-di(5-ethylhexylthienyl)benzo[1,2-b;3,3-b] dithiophene][3-fluoro-2[(2-ethylhexyl)carbonyl]thieno[3,4-b]thiophenediyl]] (PTB7-Th) blended with[6,6]-phenyl $C_{71}$-butyric acid methyl ester ($PC_{71}BM$), we identify the origin of the photo current modulation by the angle of incidence $\theta$ and the absorber layer thickness $h$.

Figure 1(a) depicts the OSC architecture comprising a PTB7-Th:$PC_{71}BM$ absorber layer, an indium tin oxide / zinc oxide (ITO/ZnO) cathode and a molybdenum oxide / silver ($MoO_3$/Ag) anode. The optical simulation of (non-polarized) sunlight propagation under oblique angles of incidence relied on the transfer matrix method,[11,12] separately considering s- and p-polarized light. The optical properties of the solar cells, such as the absorption, were then obtained by taking the mean of the respective s- and p-polarization results. The absorption within the device is proportional to the squared modulus of the sum of the forward and backward propagating complex electric field amplitude. For p-polarized light, the electric fields of the forward and backward propagating waves

[a]jan.mescher@kit.edu
[b]alexander.colsmann@kit.edu

 

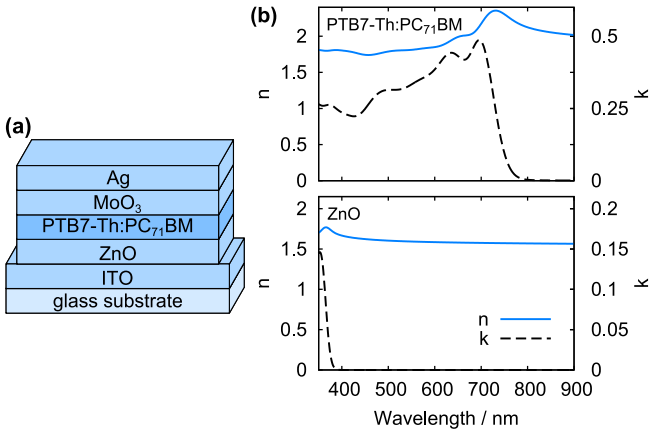


FIG. 1. (a) Schematic representation of the inverted device architecture. (b) Complex refractive indices of PTB7-Th:$PC_{71}BM$ and the nanoparticulate ZnO layer as determined by spectroscopic ellipsometry.

within the device do not have the same orientation, and hence the sum of both components has to be obtained by vector addition.[8] The complex refractive indices of $MoO_3$, Ag and ITO were taken from the literature and verified by comparing simulated and measured transmission spectra.[13–15] The complex refractive indices of PTB7-Th:$PC_{71}BM$ and ZnO, as depicted in Figure 1(b), were determined by spectroscopic ellipsometry, using a generalized oscillator model and an effective medium approximation (EMA) following the procedure discussed by Klein et al.[16] Therefore, we separately measured ~50 nm thick films of PTB7-Th and $PC_{71}BM$ with a variable angle spectroscopic ellipsometer (Woollam VASE). The data was fitted using a set of Gaussian oscillators with variable center energies, amplitudes and widths. The main fit parameter for the blend layer within the EMA was the weight ratio of the two blend materials.

In parallel, we fabricated devices on ITO coated glass ($R_{\square} \approx 13\,\Omega$/sq) which had been structured in hydrochloric acid. The substrates were subsequently cleaned in an ultrasonic bath in acetone and isopropanol for 10 min. A 30 nm ZnO electron extraction layer was spin cast from ZnO nanoparticles (Nanograde Ltd., 4000 rpm, 30 s) and annealed (80° C, 10 min). PTB7-Th (1-Material, commercial name PCE10) and $PC_{71}BM$ (Sigma Aldrich) were dissolved separately in chlorobenzene and then mixed at a ratio of 2:3. Then 4 vol% 1,8-diiodooctane (Sigma Aldrich) were added for enhanced morphology formation. The active layers were applied by spin casting. We varied the concentration of the blend in solution (18 mg/mL, 21 mg/mL and 25 mg/mL) to yield layer thicknesses of approximately 55 nm, 70 nm and 100 nm at a rotation speed of 2000 rpm. In order to obtain a layer thickness of 120 nm, the 25 mg/mL solution was spincast at 1500 rpm. The samples were annealed at 70° C for 2 hours. For the top contact, 10 nm $MoO_3$ and 100 nm Ag were deposited via thermal evaporation in high vacuum. All devices were characterized under AM1.5G illumination (100 mW/cm$^2$) from a spectrally monitored 300 W Oriel solar simulator. Current density-voltage ($J$-$V$) curves were recorded with a source measure unit (Keithley 238). For the determination of the optoelectronic properties under oblique angles, a modified rotation stage (PI Mercury C-863.11) was used. Layer thicknesses were measured with a tactile profiler (Bruker Dektak XT).

Light absorption in OSCs is ruled by thin-film interferences that in turn depend on the layer thicknesses. Therefore, we first study the impact of the absorber layer thickness on the device performance under normal light incidence ($\theta = 0°$) by fabricating a series of OSCs with different active layer thicknesses $h$ = 55 nm, 70 nm, 100 nm and 120 nm. The measured short-circuit current densities ($J_{SC}$), open-circuit voltages ($V_{OC}$), fill factors ($FF$) and power conversion efficiencies ($PCE$) are summarized in Table I. Up to an active layer thickness of 100 nm, $J_{SC}$ increases to a maximum of 15.1 mA/cm$^2$ due to enhanced light absorption. Beyond $h$ = 100 nm, $J_{SC}$ drops, yielding 14.6 mA/cm$^2$ at a layer thickness of 120 nm.

The $J_{SC}$ increase for active layer thicknesses <100 nm and its decrease for active layer thicknesses >120 nm originates from the spatial distribution of the optical field throughout the OSCs and

TABLE I. Measured electrical key performance parameters of the OSCs versus the active layer thickness $h$ under AM1.5 illumination at normal angle of light incidence.

| $h$ | $J_{SC}$ | $V_{OC}$ | FF | PCE |
|---|---|---|---|---|
| 55 nm | 11.4 mA/cm$^2$ | 772 mV | 64 % | 5.6 % |
| 70 nm | 13.3 mA/cm$^2$ | 777 mV | 63 % | 6.5 % |
| 100 nm | 15.1 mA/cm$^2$ | 771 mV | 61 % | 7.1 % |
| 120 nm | 14.6 mA/cm$^2$ | 783 mV | 61 % | 7.0 % |

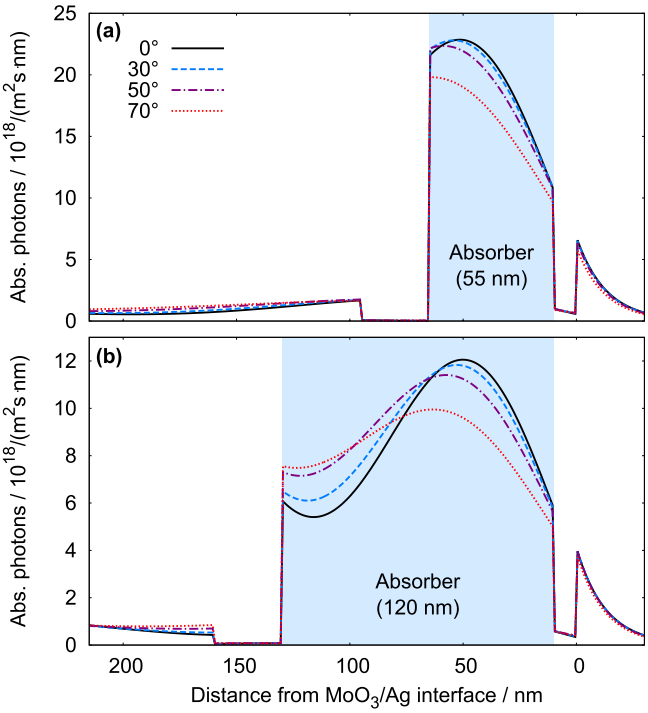


FIG. 2. Simulated spatial absorption profile throughout the OSC comprising (a) a 55 nm or (b) a 120 nm thick active layer for different angles of light incidence $\theta$. Both samples were virtually illuminated with AM1.5 white-light.

hence from the absorption profiles which are exemplified in Figure 2 for 55 nm and 120 nm thick absorber layers (solid lines). Here, we have simulated the position dependent number of absorbed photons throughout the active layer, assuming a radiant flux $\Phi$ according to an AM1.5 standard illumination. Due to the high reflection at the interface between $MoO_3$ and silver, the number of absorbed photons within the absorber layer in the very proximity to the silver anode is small but increases with an increasing distance to the anode. The white-light interferences lead to a first distinct maximum of the optical field, and thus of the absorption profile, further away from the metal anode. For normal light incidence ($\theta = 0°$) and an $h = 55$ nm thick active layer in Figure 2(a), only part of the absorption maximum is captured by the active layer. Towards thicker layers, the total number of absorbed photons $N_p$ within the active layer increases since more of the absorption maximum is captured by the active layer. For even thicker active layers (120 nm, Figure 2(b)), $N_p$ and the generated $J_{SC}$ somewhat decrease due to detrimental changes of the thin-film interferences and the optical field. This observation is very much in accordance with literature where ~100 nm thick absorber layers are often reported as optimum light harvesters for many highly-efficient photo-active polymers.[17]

However, the optimum active layer thickness changes, when receiving light at oblique angles of incidence due to a different light propagation within the active layer. We therefore exemplify the white-light absorption profile for the 55 nm and 120 nm active layers in Figures 2(a) and 2(b),

respectively, for several angles of light incidence $\theta = 0°$, 30°, 50° and 70°. Henceforth, for all simulations, we assume an effective radiant flux $\Phi^* = \Phi/\cos(\theta)$ to account for the angle dependent reduction of the sun facing OSC area to improve the visibleness of thin-film effects. For the $h = 55$ nm thick active layer, we found that an increasing angle of incidence causes a broadening of the interference pattern which in turn leads to an interference maximum shift out of the absorber layer (Figure 2(a)). Consequently, the effective total number of absorbed photons $N_p^*(\theta)$ within the active layer drops towards increasing angles of light incidence. In case of an active layer thickness $h = 120$ nm (Figure 2(b)), the interference maximum remains within the (thick) active layer even for higher angles of incidence. While the broadening of the interference pattern causes a reduction of the number of absorbed photons close to the metal anode in the 120 nm absorber layer, the number of absorbed photons close to the ITO cathode is enhanced. In total, this leads to an increase of $N_p^*(\theta)$ within the 120 nm thick active layer for angles up to 50°.

Spatial integration of the simulated absorption profiles in Figure 2 yields $N_p^*(\theta)$ under AM1.5 illumination within the active layer. The effective total number of absorbed photons $N_p^*(\theta)$ is depicted in Figure 3 as a function of the active layer thickness for different angles of light incidence. Active layers with thicknesses $h < 60$ nm exhibit a continuous decrease of $N_p^*(\theta)$ for increasing angles of incidence $\theta$. For layer thicknesses approximately between 90 nm and 140 nm, we observe an increase of $N_p^*(\theta)$ up to an angle $\theta = 50°$. For higher angles of incidence in this layer thickness regime, $N_p^*(\theta)$ is reduced due to reflection losses at grazing angles of incidence. We note that a further increase of the active layer thickness leads to capturing a second interference maximum by the absorber (data not shown here). Notwithstanding any effects of the thicker layers on the electrical properties, the considerably thicker active layers again lead to a continuous decrease of $N_p^*(\theta)$ for increasing angles of incidence as a second interference maximum is also shifted out of the active layer, where no photo-generation of charges can occur. This is in accordance with previous observations and may become important when investigating photo-active materials that can be applied in thicker layers.[7]

These observations suggest that, for absorber layer thicknesses between 90 nm and 140 nm, an oblique solar irradiation should increase the effective photo current densities of the solar cells. To verify this hypothesis, we simulated the $N_p^*(\theta)$ under AM1.5 white-light illumination versus the angle of incidence for different active layer thicknesses and compare the results with experimental data (Figure 4). Again, in order to separate the influence of the interference effects from the angle dependent reduction of the effective sun facing device area, in all experimental results, we discuss the measured effective short-circuit current densities $J_{SC}^*(\theta) = J_{SC}/\cos(\theta)$.

The measured $J_{SC}^*(\theta)$ of OSCs with an active layer thickness of 55 nm in Figure 4(a) show a continuous decrease towards higher angles of incidence, nicely reflecting the simulated shift of the interference maximum away from the cathode and hence out of the (thin) active layer. For an active layer thickness of 70 nm, we observe a less significant reduction of the effective photocurrent

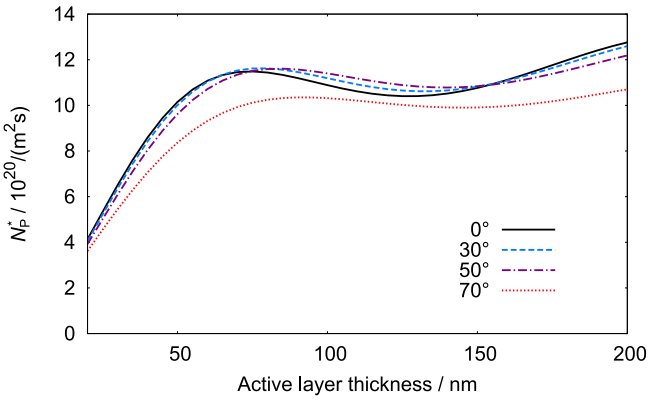


FIG. 3. Simulated total number of absorbed photons $N_p^*(\theta)$ within the active layer as a function of the active layer thickness $h$ for different angles of light incidence $\theta$ (AM 1.5 illumination).

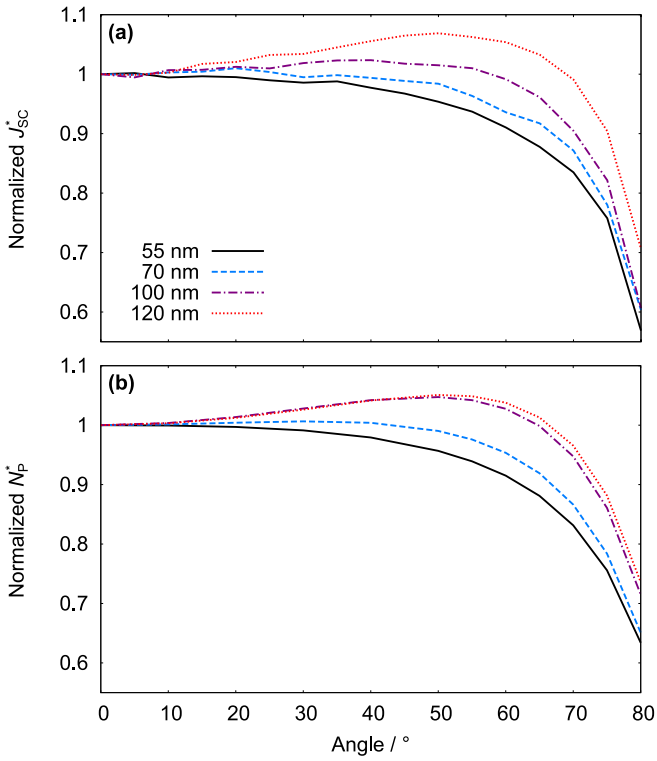


FIG. 4. (a) Measured effective short-circuit current densities $J_{SC}^*(\theta)$ and (b) simulated total number of absorbed photons $N_p^*(\theta)$ within the active layer of the OSCs versus angle of incidence $\theta$ for solar cells with active layer thicknesses $h$ = 55 nm, 70 nm, 100 nm and 120 nm.

density towards higher angles of incidence as the thicker absorber layer can still capture large parts of the shifted interference maximum. On the contrary, for OSCs with even thicker absorber layers, we observe an increase of $J_{SC}^*(\theta)$ towards intermediate angles of light incidence ($40° < \theta < 60°$). In particular, the device with a 120 nm absorber layer reaches its maximum effective photocurrent density at an angle of light incidence of 50°, being 6.9% higher than under normal incidence. For angles of incidence exceeding 60°, the effective photocurrent densities of the devices with thicker active layer also decrease, again, due to an enhanced reflection of light at the OSC surface at grazing light incidence.

Although the influence of the layer thickness is slightly more pronounced in the experimental data, both the measured $J_{SC}^*(\theta)$ in Figure 4(a) and the simulated $N_p^*(\theta)$ in Figure 4(b) show the same angle dependency. On the one hand, $N_p^*(\theta)$ and $J_{SC}^*(\theta)$ of the thinner layers (55 nm and 70 nm) decrease continuously towards increasing angle of light incidence. The thicker active layers (100 nm and 120 nm), on the other hand, lead to an increase of $N_p^*(\theta)$ and $J_{SC}^*(\theta)$ for angles up to 50°.

From this combined simulative and experimental study of the angle-dependent photon harvesting in organic solar cells we conclude that the optimum layer thickness of the absorber layer depends very much on the angle of light incidence. While OSCs in the literature are mostly optimized for normal light incidence, real-life solar cell installations that receive a lot of diffuse light or direct sun-light at oblique or varying angles, may require a different device design.

J.M. and A.M. contributed equally to this work. We acknowledge funding by the Federal Ministry of Education and Research (BMBF) under contract 03EK3504 (project TAURUS). J.M., A.M. and A.E. thank the Karlsruhe School of Optics & Photonics (KSOP) for support. The authors thank Nanograde Ltd. for providing the ZnO nanoparticles and acknowledge support by Deutsche Forschungsgemeinschaft and Open Access Publishing Fund of Karlsruhe Institute of Technology.

[1] M. Pagliaro, R. Ciriminna, and G. Palmisano, ChemSusChem **1**, 880 (2008).
[2] S.-B. Kang, Y.-J. Noh, S.-I. Na, and H.-K. Kim, Sol. Energy Mater. Sol. Cells **122**, 152 (2014).
[3] F. Nickel, T. Haas, E. Wegner, D. Bahro, S. Salehin, O. Kraft, P. A. Gruber, and A. Colsmann, Sol. Energy Mater. Sol. Cells **130**, 317 (2014).
[4] M. B. Schubert and J. H. Werner, Mater. Today **9**, 42 (2006).
[5] Z. He, C. Zhong, S. Su, M. Xu, H. Wu, and Y. Cao, Nat. Photonics **6**, 591 (2012).
[6] M. Riede, C. Uhrich, J. Widmer, R. Timmreck, D. Wynands, G. Schwartz, W.-M. Gnehr, D. Hildebrandt, A. Weiss, J. Hwang, S. Sundarraj, P. Erk, M. Pfeiffer, and K. Leo, Adv. Funct. Mater. **21**, 3019 (2011).
[7] G. Dennler, K. Forberich, M. C. Scharber, C. J. Brabec, I. Tomiš, K. Hingerl, and T. Fromherz, J. Appl. Phys. **102** (2007).
[8] A. Meyer and H. Ade, J. Appl. Phys. **106**, 113101 (2009).
[9] J. Kim, S. Jung, and I. Jeong, J. Opt. Soc of Korea **16**, 6 (2012).
[10] S. Lee, I. Jeong, H. P. Kim, S. Y. Hwang, T. J. Kim, Y. D. Kim, J. Jang, and J. Kim, Sol. Energy Mater. Sol. Cells **118**, 9 (2013).
[11] L. A. A. Pettersson, L. S. Roman, and O. Inganäs, J. Appl. Phys. **86**, 487 (1999).
[12] N. S. Christ, S. W. Kettlitz, S. Valouch, S. Züfle, C. Gärtner, M. Punke, and U. Lemmer, J. Appl. Phys. **105**, 104513 (2009).
[13] A. Abdellaoui, G. Lévêque, A. Donnadieu, A. Bath, and B. Bouchikhi, Thin Solid Films **304**, 39 (1997).
[14] E. D. Palik, "Handbook of optical constants of solids," (1998).
[15] J. Mescher, S. W. Kettlitz, N. Christ, M. F. Klein, A. Puetz, A. Mertens, A. Colsmann, and U. Lemmer, Org Electron **15**, 1476 (2014).
[16] M.F.G. Klein, G.Q. Glasner de Medeiros, P. Kapetana, U. Lemmer, and A. Colsmann, J. Photonics f. Energy **5**, 057204 (2015).
[17] F. Nickel, C. Sprau, M. F. Klein, P. Kapetana, N. Christ, X. Liu, S. Klinkhammer, U. Lemmer, and A. Colsmann, Sol. Energy Mater. Sol. Cells **104**, 18 (2012).